JAST
Journal of Aerospace Science and Technology

Pages: 119-134/ Vol. 15/ No. 2 / Summer- Fall 2022

Journal of Aerospace Science and Technology

www:jast.ias.ir

Research- Notes Article

Numerical Investigation of Aerodynamic Performance of Planar/grid Stabilizer wings at Downstream Control Surface in Transonic Flow Regime

Amir Rahni [1], **Mahdi Miralam**[2]*

1- Department of Aerospace Engineering, Amirkabir University of Technology, Tehran, Iran

2- Department of Mechanical Engineering, Shahid Rajaee Teacher Training University, Tehran

ABSTRACT

Keywords: *Grid fin; nductive roll; Aerodynamic coefficient; Static margin; Pitch*

In multi-stage missiles, stabilizer wings are responsible for stabilizing the missile. The control fins located upstream of the stabilizer wings affect the flow by spinning, which influences stability and control. One method for resolving this problem is to design stabilizer wings with less affectability against the upstream flow. The present paper deals with this issue by considering multiple planar and grid fins. The appropriate missile model is established Once validation is performed and the appropriate turbulence model and the planar and grid fins are chosen. Then, on a model with speeds of 0.6, 0.7, and 0.8 Mach, at attack angles of 0, 2, 4, and 6 degrees, and with control fins, variation at angles of 0, 1, 3, and 6 degrees, the aerodynamic coefficients, as well as the effects of the upstream stabilizer wings, are investigated in pitch and roll modes at an appropriate trim angle. The obtained results indicated that the grid fin downstream of the control surfaces would be less affected due to its physical nature. Thus, the lower capacity of the control surface would be used for control during the flight, which would significantly facilitate the process of designing.

Introduction

Grid fin is an aerodynamic control surface, the outer frame of which includes an inner lattice consisting of thin surfaces intersecting the small chord. In contrast to the conventional two-sided fins, which are aligned with the airflow in a parallel direction, grid fins are mounted vertically on the airflow by the passage of the air moving forward through the lattice cells. In recent years, the better maneuverability of grid fins at supersonic and subsonic speeds and high attack angles has been highly regarded.

A pervasive problem in tail-controlled aircraft is the large hinge moments, which can be considerably reduced by the use of grid fins. The main advantage of the grid fins over the conventional two-sided fins is their small chords. Therefore, grid fins produce smaller hinge moments, resulting in reduced operator size. The stall in grid fins occurs at higher angles than in planar fins. Hence, it is better to use grid fins in

1 PhD Candidate

2 Assistant Professor (Corresponding Author) **Email:** * m.mahdi@sru.ac.ir

DOI : 10.22034/jast.2022.245863.1033

Submit: 31. 08. 2020/ Accepted: 12 08. 2022

Print ISSN:1735-2134 Online ISSN: 2345-3648

aircraft that require high maneuverability. Consequently, grid fins are advantageous as they occupy smaller space and can easily be mounted on the aircraft during transportation and storage.
Studies conducted by Washington and Miller[1] on two grid fins in a wind tunnel showed that the more the density of the fin's lattice is, the higher its normal force will be. However, a reduction in the normal force occurs in transonic and supersonic areas.
Washington and Miller [2] investigated different models of grid fin in the wind tunnel and 3 flight tests, the results of which indicated the improved performance of the grid fin at higher attack angles and Mach numbers as well as a 25% reduction in drag force of the grid fins. This research also investigates the effect of lattice density and span variations. The results showed that increasing the density and span led to an increased normal force. On this basis, the drag of the surfaces as well as other aerodynamic features could be significantly reduced by simply forming the outer cross-section and reducing the wall's thickness or its dependent combination.

DeSpirito and Sahu [3] investigated missiles with canards and fins using CFD (computational fluids dynamics). They found out that the interfering moment produced by the fins is less than that produced by the canard in grid fins. Hughson et al. [4] studied the supersonic flow through latticing on the grid fins and using CFD, which indicated that under the supersonic Mach number, a vertical compressive wave is formed behind the lattice cells. Therefore, the flow rate within the cells is reduced due to the compressive wave within the lattice, effectively serving as an obstacle to the flow. Finally, a vertical compressive wave is developed in front of the grid fin, increasing the associated drag. At higher speeds, the lattice swallows this compressive wave, resulting in reduced drag.

Zeng et al. [5] conducted some studies to reduce the drag in grid fins. The results indicated that the drag gradually increased when the Mach number approached the transonic regime. However, a further increase in the Mach number, namely from transonic to supersonic conditions, led to a relative reduction in drag. The researcher believed this could be attributed to the flow halt within the lattice cells in transonic conditions. Using CFD, Munawar [6] compared the aerodynamic performance of the grid and planar fins. His investigations showed that at high attack angles and Mach numbers, the grid fin performs better than the planar fin. Also, the grid fin's hinge moment was much less than the planar fin. Besides, the amount of force for the grid fin was more than that for the planar fin. Bak [7] investigated the grid fin experimentally and numerically in a wind tunnel and subsonic area. Accordingly, he concluded that the grid fin had better performance at high attack angles and speeds, and the maximum difference between the numerical and experimental results occurred at an attack angle of 5 degrees.

Kless and Aftosmis [8] studied grid fins using the Cartesian-Euler solution. They performed the simulation on 12 different Mach numbers at attack angles of 0-15 degrees and in 6 different geometries. The final lattice included 7-8 million cells. In this research, there was a good consistency for the Mach numbers more significant than 1 in the simulation and the wind tunnel. Another finding of this research was that the grid fin with a backward angle exhibited the highest pitch moment in the simulation and experiments. Likewise, Prashanth et al. [9] conducted numerical and experimental studies on the grid fins of G16 missiles. They showed that at high attack angles, regarding the fact that the CN/CL/CA difference had been reduced, the L/D performance was improved, and also the drag force was reduced.
Overall, the grid fins performed better at high attack angles and supersonic speeds. Furthermore, in the same years, the use of this type of fins in the field of aircraft control was taken into consideration (Landers et al. [10]; DeSpirito et al. [11]; DeSpirito et al. [12]). As an example of the control application of this type of fins, the use of it as a stabilizer can be mentioned (Pruzan et al. [13]; DeSpirito et al. [14]; Khalid [15]).
Ledlow et al. [16] showed much lower hinge moments than planar fins, which allows for using smaller actuators for fin control. However, the major drawback of grid fins that has prevented them from seeing more applications in missile control is the high drag associated with the lattice structure, which is substantially larger than that of a comparable planar fin.
In recent years, aerodynamic research has been conducted by DİNÇER [17]. It has been concluded that the web and frame thickness-related parameters have a small effect on normal force and bending moment coefficients within the design space explored in this thesis. The important

parameter is also assessed for each aerodynamic coefficient. This is a procedure that can be applied to various design problems as well.

The present paper is aimed to compare the aerodynamic coefficients of two types of planar fins with one type of grid fins as stabilizer fin in a two-stage aircraft. For this purpose, it was attempted to find an appropriate turbulence model for numerical simulation after validation. By calculating the normal force coefficient and pitching moment of each type of fin, the grid fin was selected with a normal force coefficient close to the planar fins. Finally, these three fins were added to the aircraft separately. Then, the aircraft's aerodynamic behavior in the three states was studied and compared with each other.

Governing equations

The equations governing the averaged Navier-Stokes equations flow are the energy and Reynolds equations, which have been separated using the finite volume method:

$$\frac{\partial}{\partial t}\int_v W\mathrm{dV} + \oint [F-G]dA = \int_v H\mathrm{dV}$$

$$W = \begin{Bmatrix} \rho \\ \rho u \\ \rho \mathcal{V} \\ \rho w \\ \rho E \end{Bmatrix}, \quad F = \begin{Bmatrix} \rho V \\ \rho V u + pi \\ \rho V \mathcal{V} + pj \\ \rho V w + pk \\ \rho V E + pv \end{Bmatrix}, \quad G = \begin{Bmatrix} 0 \\ \tau_{xi} \\ \tau_{yi} \\ \tau_{zi} \\ \tau_{ij} V_j + q \end{Bmatrix} \tag{1}$$

Where W is the vector of survival variables, and F and G indicate inviscid and viscid flux vectors, respectively. Also, H is the source terms vector (Due to the lack of Body force, the value of H is zero.), V is the cell volume, and A is the cell's surface area. The inviscid flux vector (F) is assessed using the standard upstream flux difference (Hoffman [18]).

As an ideal gas, the air was considered the working fluid, and the flow was deemed steady. Separation of the equation was performed using the finite volume method and with second-order accuracy. The SIMPLE algorithm was used to couple the velocity and pressure. Regarding the importance of the flow beside the wall, latticing was performed using the hybrid method, and a boundary layer was created near the lattice wall. Thus, the flow was solved up to the wall's side, and the wall's functions were not applied. For the outer boundary, the far-field pressure condition was used. This boundary condition is non-reflective, i.e., the shocks are not reflected in the field non-physically (Cai [19]; Theerthamalai and Balakrishnan [20]).

The $k-\omega$ model has been used to simulate the turbulent flow with respect to the Reynolds number range in the present problem. The continuity equation is as follow:

$$\frac{\partial \rho}{\partial t} + \nabla.\left(\rho \vec{V}\right) = S_m \tag{2}$$

In Equation (2), S_m is the source expression whose value is considered zero.

The Momentum equation is shown in Equation 3.

$$\frac{\partial}{\partial t}\left(\rho \vec{V}\right) + \nabla.\left(\rho \vec{V}\vec{V}\right) = -\nabla P + \nabla.(\bar{\bar{\tau}}) + \rho\vec{g} + \vec{F} \tag{3}$$

In Equation (3), P is the static pressure (Pa), $\overrightarrow{\rho \mathrm{g}}$ is the gravitational force (Kg $/m^2.s^2$) and $\vec{F}$ is the external force (N), which is assumed to be zero. $\bar{\bar{\tau}}$ is the stress tensor defined as follows:

$$\bar{\bar{\tau}} = \mu[\left(\nabla \vec{V} + \left(\nabla \vec{V}\right)^T\right) - \frac{2}{3}\nabla.\overrightarrow{V}, I] \tag{4}$$

Where μ is the molecular viscosity (kg /m.s) , I is the unit tensor , $\nabla \vec{V}$ is the matrix form of the velocity gradient tensor, and $\left(\nabla \vec{V}\right)^T$ is transpose of the $\nabla \vec{V}$. The $k-\omega$ SST equations are presented as follows:

The matrix form of the velocity gradient tensor

$$\frac{\partial}{\partial x_i}(ku_i) = \frac{1}{\rho}\left[\frac{\partial}{\partial x_i}\left[\Gamma_k \frac{\partial k}{\partial x_j}\right] + \widehat{G_k} - Y_k + S_k\right] \tag{5}$$

$$\frac{\partial}{\partial x_j}(\rho\omega u_i) = \frac{1}{\rho}\left[\frac{\partial}{\partial x_j}\left[\Gamma_\omega \frac{\partial \omega}{\partial x_j}\right] + \widehat{G_\omega} - Y_\omega + D_\omega + S_\omega\right] \tag{6}$$

In the above equations, $\widehat{G_k}$ represents the generation of turbulence kinetic energy due to mean velocity gradients, G_ω represents the generation of ω, $D_\omega$represents the cross-diffusion term, S_ω , S_k are user-defined source terms, Γ_ω , Γ_k

represent the dissipation rates of ω and k due to turbulence:

$$\Gamma_k = \mu + \frac{\mu_t}{\sigma_k} \quad (7)$$

$$\Gamma_\omega = \mu + \frac{\mu_t}{\sigma_\omega} \quad (8)$$

Where σ_k and σ_ω are the Prandtl numbers for ω, k respectively, and μ_t is turbulence viscosity.
For convergence in CFD simulations, initial guessing is required. In this research, there are two ways for this purpose, which are Standard initialization or Hybrid initialization. The analyses showed that using Standard initialization with FMG command had better stability in the solution.

Validation

The aerodynamic coefficients were extracted using the CFD method. The 3D Navier-Stokes equations of compressible flow were used along with the turbulence model and energy equation for simulating the turbulent flow. FLUENT V.15 software was selected as a solver of the flow for sampling the flow phenomenon. The governing equations were solved using the finite volume method and the hybrid lattice. In the present paper, the flight test results and comparison of the aerodynamic coefficients were used to obtain and select the proper turbulence model.

Validation model conditions

Abate and Duckerschein [21] conducted flight tests on missiles with grid fins at subsonic and transonic flow. These flight tests were performed in ARF (Aeroballistic Research Facility) by the US Air Force Ammunitions Research Center. The geometry of the validation in the present paper was used for simulation and comparison of the obtained results.

This model has a length of 16D, a diameter of 1D, and a Tangent-Ogive nose with a length of 3D. The fins are installed on the body as a cross at a 14.441D distance from the missile tip. The software considered all the given conditions in the numerical simulation. A temperature of 22 ± 1ºC was applied for this test, but the static pressure, the center of mass, and density varied in each test concerning the velocity of the test. The same conditions were applied for simulation in accordance with Table 1.

Table 1 The conditions of flight test

Pressure (Pa)	Density (kg/m^3)	Center of mass (length)	Mach number
103450	1.2012	0.4778	0.574
103650	1.2030	0.4763	0.744
103600	1.2030	0.4765	0.817

In the present paper, the diameter of the model was considered equal to 25.4 mm, assuming that the length of the aircraft was 406.4 mm. Figures 1 and 2 demonstrate the prepared model. Using ANSYS software, a hybrid grid was created in the flow field around the model. Near the aircraft's wall, the boundary layer grid was created, so that the distance of the first node from the body was 0.001 mm, with ten layers. Figure 3 demonstrates the flow field and unstructured grid created around the model. The density of the grid around the model is shown in this figure. The boundary layer grid created near the nose is shown in Figure 4.

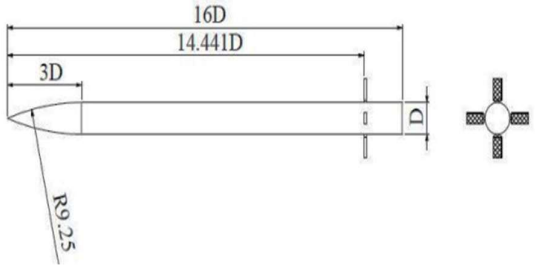

Figure 1. The total model aircraft simulated with the grid fin in gambit.

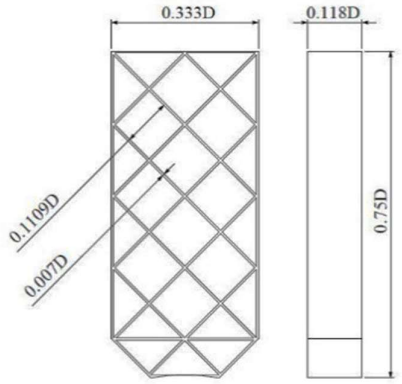

Figure 2. The grid fin model.

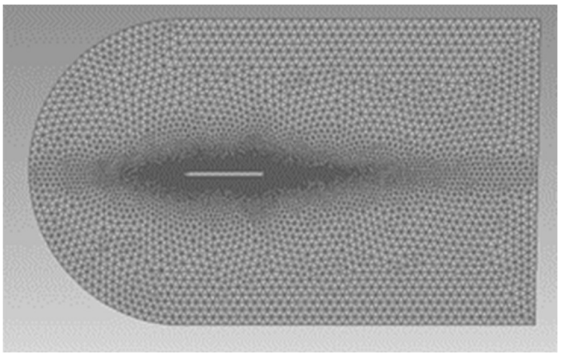

Figure 3. The flow field around the model.

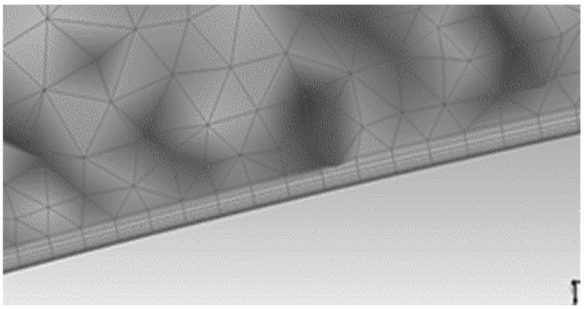

Figure 4. The prism grid near the nose.

Validation results

Simulation of the model was performed with Mach numbers of 0.574, 0.744, and 0.817 at angles of attack in 0, 2, 4, and 6 degrees. This simulation was performed using FLUENT software for different turbulence models, including K-ω-SST, K-ε-St, and K- ε -Re (K-epsilon-Realizable). Besides, the CFX software was used with SST (Shear Stress Transport) turbulence model for more precise simulation. The model was considered symmetric to reduce the calculations. The calculations were continued up to the error of less than 10-4 to achieve convergence.

After meshing and defining the boundary conditions, the reference model was analyzed for three Mach numbers of 0.574, 0.744, and 0.817, and different angles of attack. Figure 5 represents the normal force coefficient variations in accordance with the angles of attack for the Mach number of 0.744 for different turbulence models. For all of these states, the behavior of the normal force coefficient C_N was linear with the angles of attack. Thus, it would be better to investigate the results using the slope of the diagrams $C_{N\alpha}$.

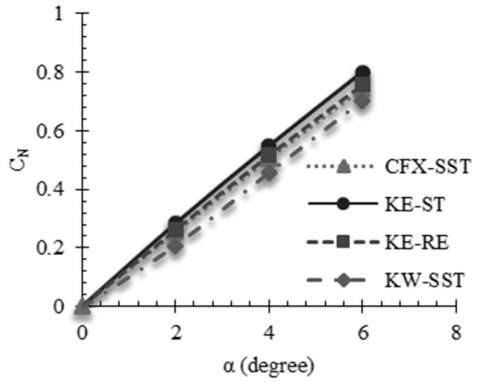

Figure 5. The normal force coefficient in Mach 0.744.

The values of $C_{N\alpha}$ for different Mach numbers are presented in Table 2. This table also represents the results of the flight tests from Abate and Duckerschein (2000). The obtained values are well consistent with the flight test results. For a more precise investigation, the error percentage of each state was compared with the experimental results, which are presented in Table 3. The maximum error value is about 11%, and the rest are less than this value. Thus, acceptable results could be obtained by selecting the appropriate grid using different turbulence models. A more precise investigation and comparison between the error percentages indicated that using ANSYS FLUENT software with the K-ε-St turbulence model would yield the lowest error value compared to the experimental results. The error value in this state was less than 2%. The present paper aimed to design a fin as a stabilizer and sought more static stability. Therefore, the fin's normal force was used more, and the axial force was not taken into account.

Table 2. The results of CNα (rad^{-1})

Fluent K- ε -Re	Fluent K- ε -ST	Fluent K- ω	CFX-SST	Abate (2000)	Mach Number
7.6433	7.5425	7.2651	7.1562	7.630	0.574
7.2479	7.7179	6.7784	7.1046	7.620	0.744
6.9958	7.2946	6.7609	7.4198	7.390	0.817

Table 3. The percentage error of CNα (rad^{-1})

Fluent K- ε -Re	Fluent K- ε -ST	Fluent K- ω	CFX-SST	Mach Number
0.1%	1.1%	4.7%	6.2%	0.574
4.8%	1.1%	11%	6.7%	0.744
5.3%	1.3%	8.5%	0.4%	0.817

Figure 6 shows the Mach number distribution in the flow field around the grid fin for a Mach number of 0.574 and an attack angle of 2 degrees.

The fin's cells served as a nozzle so that the flow velocity within the cells was increased, and the maximum value of Mach number reached 0.7169. In the front wall of the cells, the stationary point is formed, and the flow separation occurs in the back part.

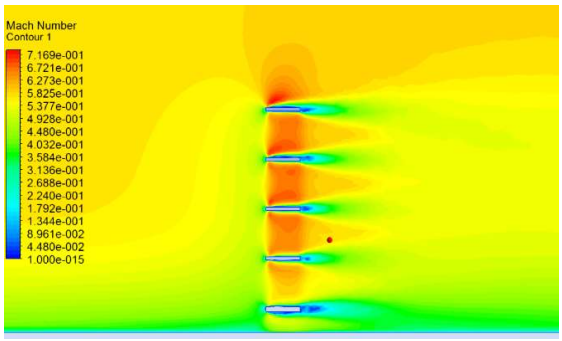

Figure 6. The contour of Mach number at symmetry plan of grid fin for M=0.574 and α=2°

Figure 7 shows the distribution of Mach number at the symmetry plane of the model and around the grid fin under flight conditions of M=0.744 and an attack angle of 2 degrees. In this figure, the value of the Mach number within the cells has been increased, the maximum of which has reached 1.008. Consequently, choking occurs inside the cells, and the vertical waves form inside the grid fin's cells. By increasing the flight Mach to 0.814, due to the flow choking within the cells, it has overflowed around the fin, and the maximum Mach number has occurred at the outer surface of the fin (Figure 8).

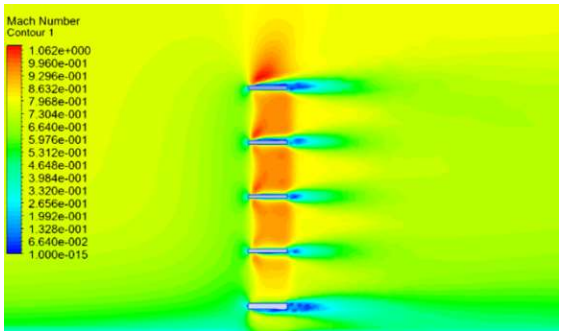

Figure 7. The contour of Mach number at symmetry plan of grid fin for M=0.744 and α=2°

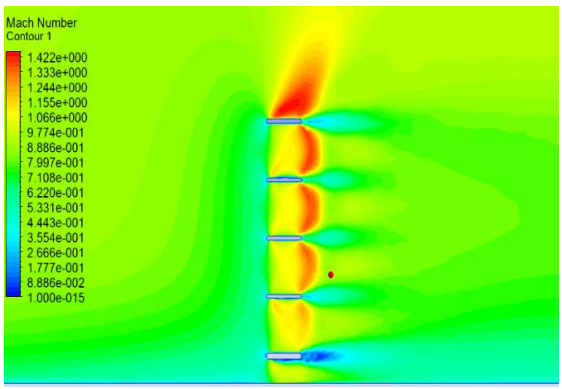

Figure 8. The contour of Mach number at symmetry plan of grid fin for M=0.817 and α=2°

Geometry and design of simulation model

In two-stage aircraft, which are the subject of this paper, initially, overcoming the inertia force is the responsibility of the booster, which is used in the first stage of the flight. Then, the main engine enters the circuit and creates the driving force for other parts. One of the requirements of flight in these aircraft is the presence of static stability. Static stability is examined and measured by a variable called static margin. The stabilizer fin is responsible for creating a moment against the moment created by the mass relative to the aircraft's tip. An exact design of the stabilizer fin can help obtain the appropriate static margin and establish static stability.

Shape of the main model

Here, three models of aircraft with different stabilizer fins are investigated, and their performances with various properties are compared with each other in order to find the best stabilizer. Figures 9, 10, and 11 show the three selected models.

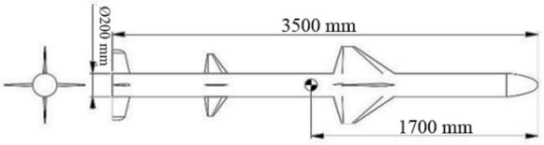

Figure 9. The general model with PL1 fin

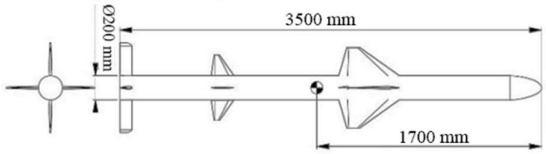

Figure 10. The general model with PL2 fin

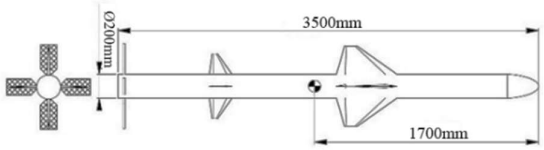

Figure 11. The general model with Grid fin

The main model selected in the present paper has a length of 3500 mm, a diameter of 200 mm, and a mass center of 1700 mm from the aircraft's tip size. The location of the wing and control fin is the same in all the models. Also, the location of the stabilizer fin is the same in all three models, and the middle of their thickness has been considered the fins' location. In this aircraft, first, a simulation was performed without the stabilizer fin to calculate the value of the pitching moment and normal force required for static stability. Next, the stabilizer fin PL1 was designed regarding the obtained results. Afterward, a model of the fin PL2 was designed to reduce the created pitching moment. Finally, a grid fin that could meet these requirements was modeled.

Geometry of stabilizer fins

The designed PL1 fin had a cross-section of Naca0015 with a height of 202 mm, chord length of 140.71 mm, and thickness of 8.12 mm. Therefore, the length of the chord with a 77.12° angle was reduced to 100.57 (Figure 12).

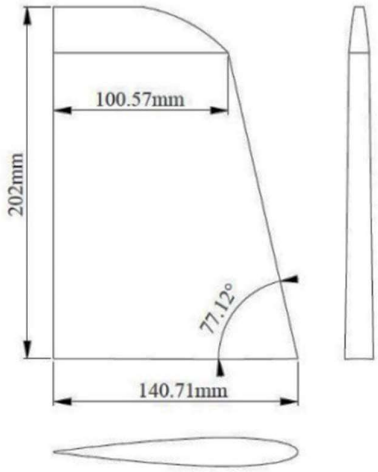

Figure 12. The PL1 fin model

The designed PL2 fin had a cross-section of Naca0015 with a height of 267.6 mm, a chord length of 100 mm, and a thickness of 12.04 mm, as shown in Figure 13. However, the chord length was not reduced in this model.

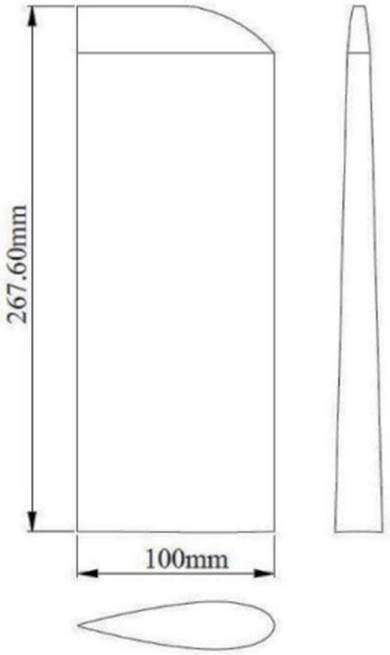

Figure 13. The PL2 fin model.

The selected grid fin was optimized using Bak's method (2010). Such calculations derived a model with a height of 251.29 mm, chord length of 135.37 mm, and thickness of 16 mm. The geometry of this optimized grid fin is shown in Figure14.

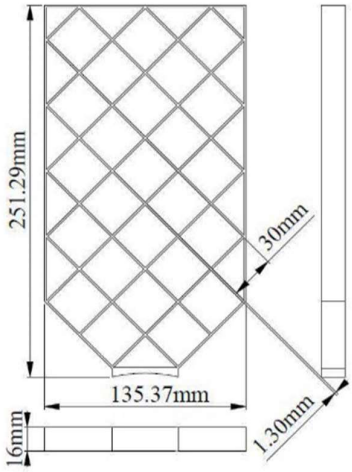

Figure 14. The grid fin model

In order to investigate and compare the normal force of the designed fins, first, a semi-cylindrical field with a spherical nose was considered. Next, each fin was separately examined at Mach numbers of 0.6, 0.7, and 0.8 and angles of 0, 2, 4, 6, 8, and 10 degrees. The results obtained for the normal force coefficient variations in accordance

with the attack angle in Mach numbers of 0.6, 0.7, and 0.8 are presented in Figure 15, 16, and 17, respectively. By comparing the normal force coefficients of these three fins, it can be concluded that at low attack angles, the diagrams are matched. However, once the attack angle is increased, the normal force coefficient value of the PL1 would be less than that of the Grid fin, and both of these fins would be weaker than the PL2 model. Therefore, this difference is less than 10%.

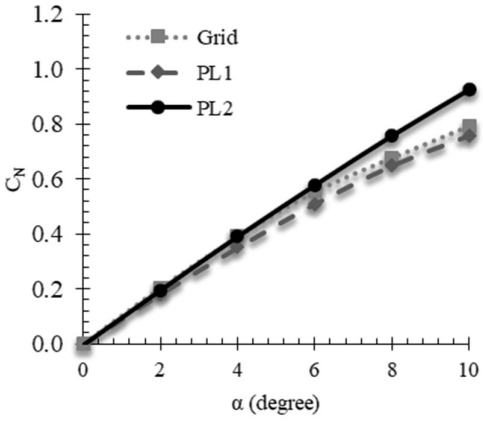

Figure 15. The normal force coefficient in Mach 0.6.

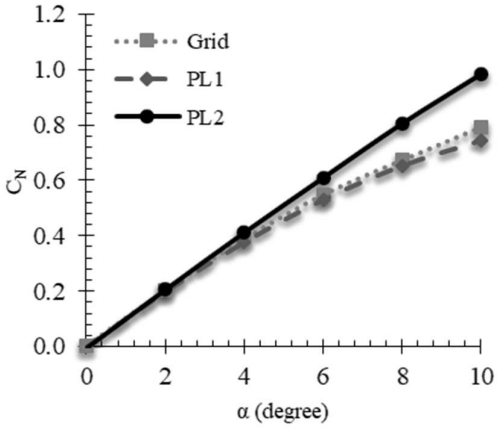

Figure 16. The normal force coefficient in Mach 0.7.

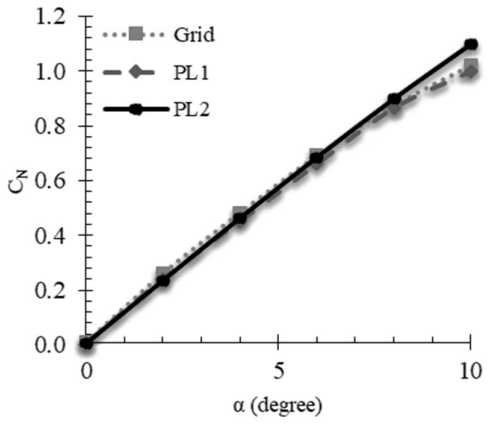

Figure 17. The normal force coefficient in Mach 0.8.

Meshing

One of the simulation's most essential steps in CFD problems is producing an appropriate mesh. The present paper had a complicated geometry, and it was impossible to create an organized mesh. Also, an unorganized mesh commonly lacks sufficient precision. Also, the viscous forces near the body were of great importance. Therefore, a hybrid mesh was used in this work as in the validation model. The mesh around the body can be used from the unstructured mesh to reduce the number of cells. Examples of the mesh quality around the wing in different states are presented in Figure 18, 19, and 20.

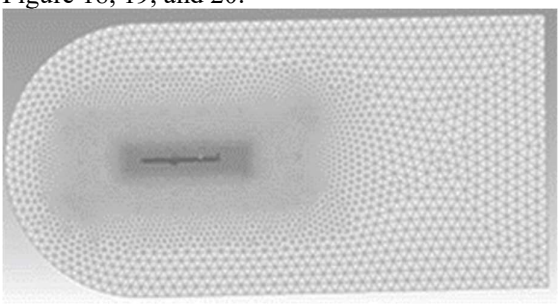

Figure 18. Mesh quality at the cross-section parallel to the axis.

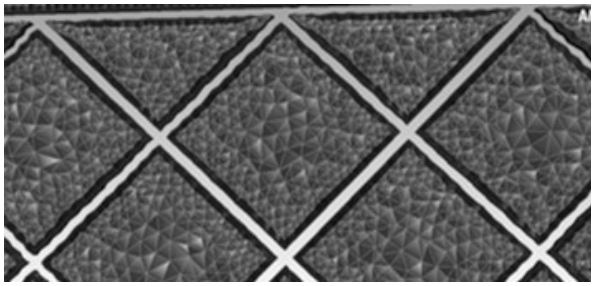

Figure 19. Mesh quality inside cells of the wing.

Figure 20. Prism mesh near the wall

A numerical analysis was performed to investigate this problem with different numbers of cells. By increasing the mesh density, values of the coefficients varied so that these variations were continued up to 3846532 cells in the planar fin model. Above this number, the variations were not tangible since they reached less than 1%. Hence, meshing with a density of 3058739 was considered the desired density for this type of fin. The above results at a Mach number of 0.6 and attack angle of 4 degrees in planar fin are shown in Figure 21 and 22 for normal force and axial force coefficients, respectively.

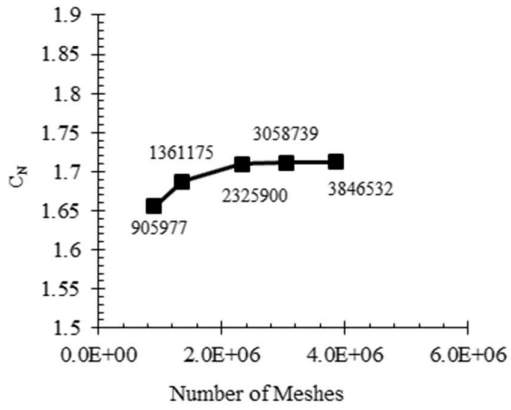

Figure 21. The variation of normal force coefficient planar fin model with mesh number.

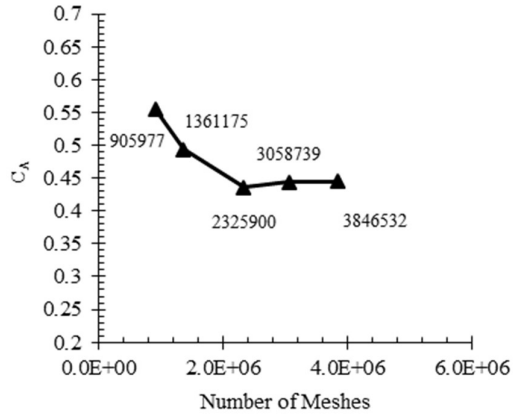

Figure 22. The variation of axial force coefficient planar fin model with mesh number.

The same procedure was performed for the aircraft model with the grid fin because it commonly has more cells due to its bigger volume than other models. Finally, the mesh with a density of 4958487 was selected for the grid fin model. The above results at a Mach number of 0.6 and an angle of attack of 4 degrees in grid fin are shown in Figure 23 and 24 for normal force and axial force coefficients, respectively.

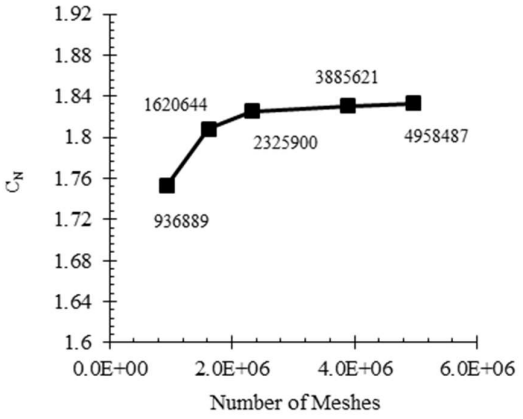

Figure 23. The variation of normal force coefficient grid fin model with mesh number.

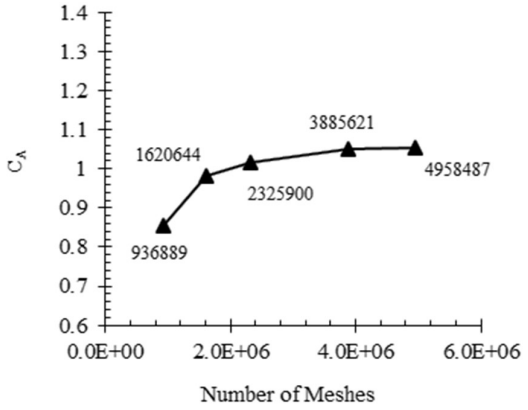

Figure 24. The variation of axial force coefficient grid fin model with mesh number.

Investigating Results

In order to investigate the simultaneous effect of control and stabilizer fins on an aircraft's aerodynamic and stability coefficients, the numerical analyses were performed at pitch and roll channels at different Mach numbers and attack angles. In all the analyses, the air was considered the ideal gas under standard conditions $P = 1$ atm and $T = 300$ K. All the separations were of second-order, and the analyses performed were reliable.

In the first step, the fins' angles were set to create positive pitch moments, meaning that the aircraft's nose was lifted upward. The simulation was performed at a certain pitch angle for three different stabilizer fins at flight Mach numbers of 0.6, 0.7, and 0.8 and angles of attack of 0, 2, 4, and 6 degrees. Figure 25 represents the value of the normal force coefficient applied on the aircraft at a fin angle of 0 and a Mach number of 0.7 for different angles of attack. For all three stabilizer fins, the behavior of the normal force coefficient in accordance with the attack angle was linear. The slope value of the diagram for the grid stabilizer fin was higher than that of the planar fins. The planar stabilizer fin with a bigger span (PL2) exhibited a higher slope of the diagram for the normal force coefficient than the fin with a bigger chord value (PL1). The normal force coefficient variations for Mach numbers of 0.6 and 0.8 were similar to those of Mach number of 0.7. Although the normal force coefficient of the stabilizer fin PL2 (Figure 16) was bigger than the two other states individually, the effects of vortex shedding caused by the control fin and the body weakened this fin's performance in comparison with the two other models. The normal force coefficient value of the grid fin indicates the less affectability of this type of fin compared to the planar fins.

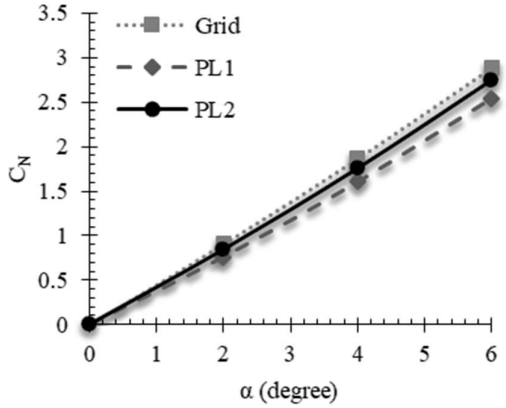

Figure 25. The Normal force coefficient variations at 0º pitch (M=0.7).

Figure 26 shows the pitch moment coefficient around the center of mass. Since the angle of control fins was zero, for all three models, the pitch moment coefficient value was about zero at an angle of attack 0. With the increase in the angle of attack, the value of the moment produced by the grid stabilizer became negative, and the aircraft's nose was directed downward. For the PL1 stabilizer, the aircraft was still unstable up to the angle of attack of 5 degrees, and the PL2 model was unstable up to the angle of attack of 2 degrees. Due to the geometrical nature of the stabilizer fins and their capability of being affected by the upstream flow, a significant difference could be observed in the value of the pitch moment produced in the aircraft.

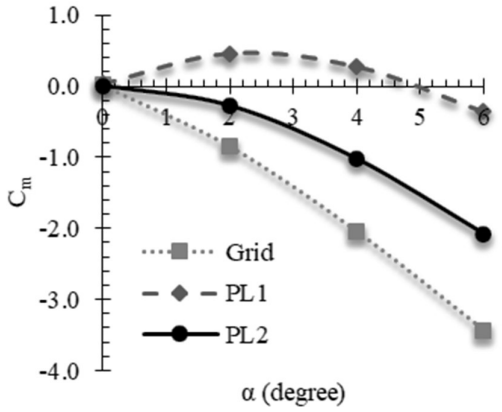

Figure 26. The pitch moment coefficient variation at 0º pitch (M = 0.7).

The high slope in the model grid diagram indicates better stability of this model compared to

the others. Of course, if the moment coefficient slope exceeds a specific limit, it will make the aircraft lag. A good measure for examining static stability is the static margin number. Eq. (2) represents the static margin number.

$$ST = \frac{X_{Cp} - X_{Cg}}{D} \quad (2)$$

In order to prevent the lag of aircraft responses, having a static margin equal to unity would be one of the best criteria. Table 4 represents the values of the static margins of different models at an angle of attack of 4 degrees and different Mach numbers. The model PL1 is unstable for all three Mach numbers. The stability value for the PL2 model is a relatively small number, while the model Grid has the best stability at all the given speeds.

Table 4 Static margins in different Mach numbers

M = 0.8	M = 0.7	M = 0.6	Fin	Alpha
-0.24	-0.2	-0.21	PL1	α = 4
0.4	0.6	0.53	PL2	
1.2	1.0	1.0	Grid	

Usually, for an aircraft to produce the lift force, regarding the aircraft's geometry and mass, an angle of attack is considered such that the produced lift force is equal to the mass value. Therefore, the trim at an angle of attack 0 is meaningless. The value of the trim angle depends on the aircraft's flight Mach number. If the trim angle for Mach number of 0.7 is equal to 1 degree, shown in Figure 27, the moment value at an angle of attack of 1 degree will be negative only for the model Grid and positive for the two other models. Thus, trimming the aircraft will be possible only in the Grid mode. For this reason, the control fin's angles are changed by 3 degrees. Therefore, they produce a positive pitch moment around the center of mass. For this mode, all three models were simulated at different angles of attack. Figure 27 shows a diagram of the pitch moment coefficient variation in accordance with the angle of attack for the three models. The notable point is that at an attack angle of 0 degree, the moment value for model PL1 is still zero. However, the total pitch moment is positive for the two other models due to the control fin's moment. The grid fin model reaches the trim at an attack angle of 1 degree, while the trim for model PL2 occurs at an attack angle of 4 degrees. To further investigate this state, a 6˚pitch was applied to the model by changing the control fin's angle to 6 degrees. Figure 28 shows the pitch moment diagram for this state with a Mach number of 0.7.

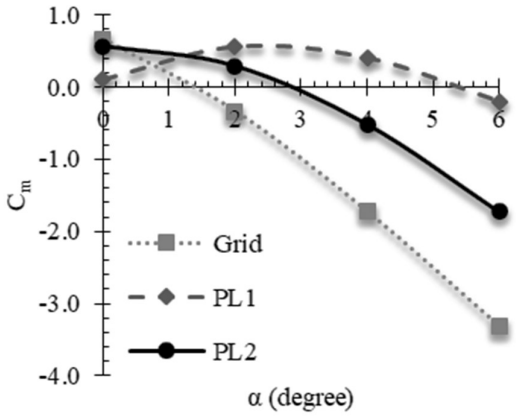

Figure 27. Pitch moment coefficient variations at 3˚ pitch (M=0.7).

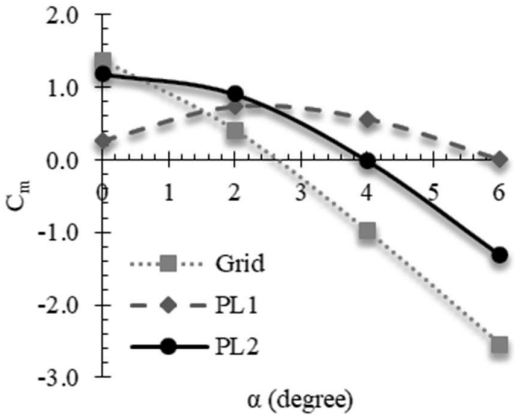

Figure 28. Pitch moment coefficient variations at 6˚ pitch (M=0.7).

In this state, the model Grid will reach trim at an angle of 2.5˚ and 6˚ pitch. Besides, other models have undesirable statuses in terms of stability, and the model PL1 will reach trim at the angle of 6 degrees. The best choice in these investigations was to have a trim with minimum deflection. It is shown that model Grid will reach trim earlier than other models. All of these cases were investigated at Mach numbers of 0.6 and 0.8, which led to the same results.

In aircraft with control fins installed in the middle section and stabilizer fins installed at the end of the aircraft, shedding of the vortexes of the fins on the stabilizers usually causes the input flow of the stabilizers to enter the stabilizer fins at an

angle other than the free-angle. Therefore, in addition to the pitch moment, the roll moment might also be produced by the stabilizers. Regarding the aircraft's low inertia moment around the longitudinal axis, the small value of the roll moment can be dangerous during the flight. Hence, it is necessary to examine the produced roll moment value in each stabilizer in different conditions.

Figure 29 shows the roll moment coefficient value for different fin angles for the three models. This diagram shows the low value of the induced moment in the model Grid, created due to the pitch effect. Afterward, the model PL2 has the least induced moment up to the deflection angle of 3 degrees. Furthermore, model PL1 has the highest induced moment in the pitch channel due to its larger chord surface than the two other models. There is an essential point about jumping of the diagram in model PL2, which is attributed to the effect of the upstream flow of the control fin on the PL2 stabilizer. Figure 30 shows the diagram of the induced roll moment at a Mach number of 0.7. This diagram is the same as the diagram of the Mach number of 0.6, in which the model Grid has the minimum affectability. The jumping of the diagram is also seen in model PL2. Therefore, for a more thorough investigation of this jumping, the effect of the Mach speed flow on the stabilizer wing is presented in Figure 31. This figure has been extracted from FLUENT software.

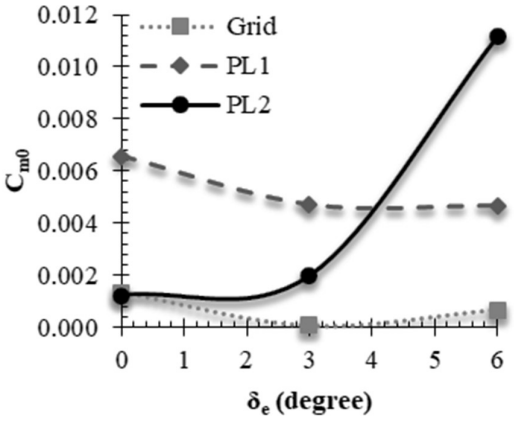

Figure 29. Diagram for inductive roll moment coefficient at Mach number of 0.6.

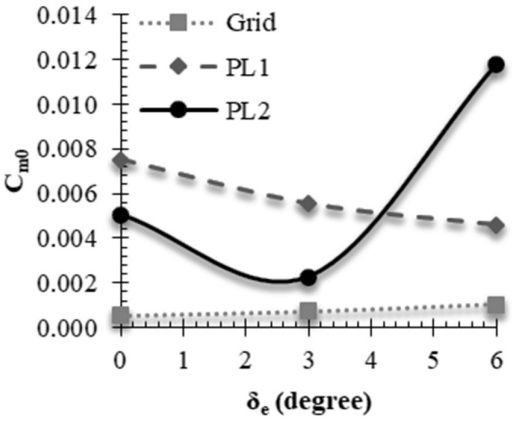

Figure 30. Diagram for inductive roll moment coefficient at Mach number of 0.7.

Figure 31 shows the Mach number streamline on the control fin up to the end fin of model PL2. As a result of the collision of this downwash with the end stabilizer wing, an inductive roll moment is created on the wing's chord. Then, with an increase in the deflection of the control fin to 6 degrees, the Mach number streamline is changed. As seen in Figure 32, the upstream flow of the stabilizer wing, which is disrupted by the control fin, collides with one side of the wing, which imposes a one-sided force on the stabilizer wing, leading to the jumping of the inductive roll moment coefficient's value in Figure 29 and 30.

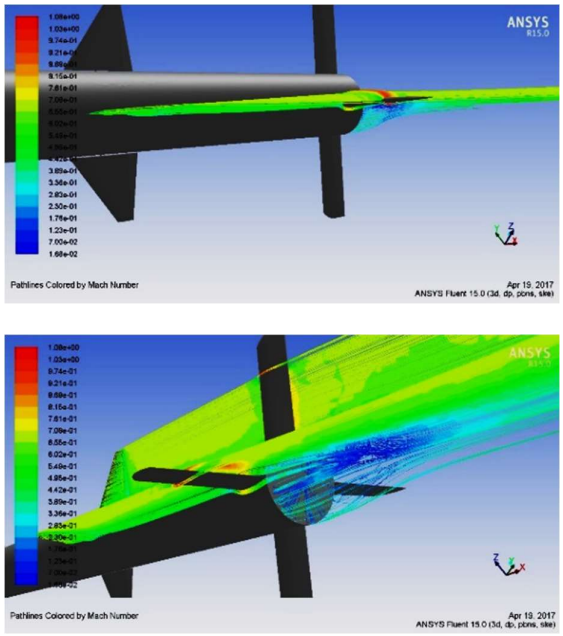

Figure 31. Diagram for Mach number of effect of upstream flow at a speed of 0.7 Mach: a=0, D=3.

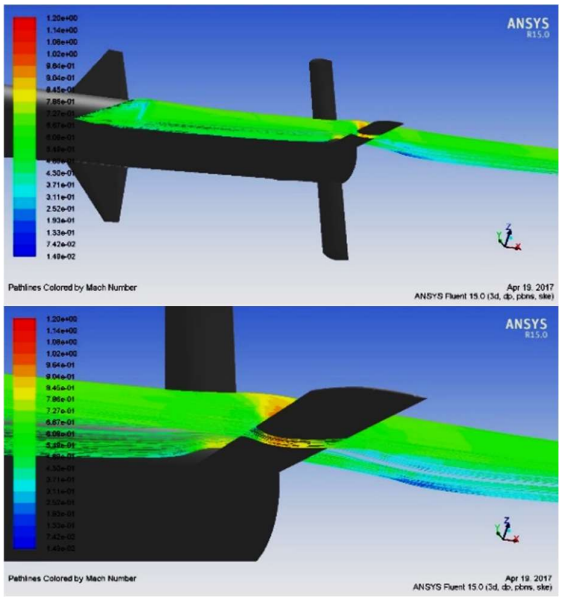

Figure 32. Diagram for Mach number of upstream flow at a speed of 0.7 Mach: a=0, D=3.

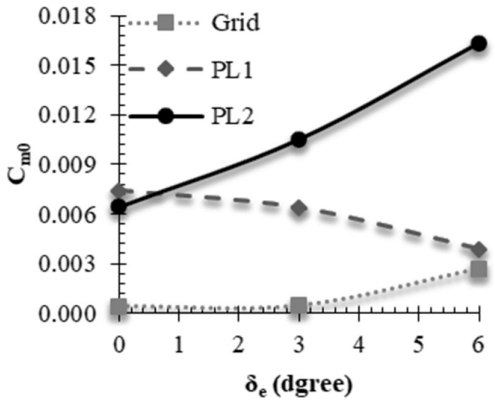

Figure 33. Diagram for inductive roll moment coefficient at a Mach number of 0.8.

Figure 33, which shows the induced roll moment coefficient at a Mach number of 0.8, confirms the superiority of model Grid as in the previous speeds. On the other hand, according to the results obtained for the two previous speeds, the increase in this coefficient in model PL2 is due to the small chord of this wing. As a result, the flow jumps due to its high speed and creates a bigger peripheral force and, consequently, a bigger inductive moment.

Speeds of 0.6, 0.7, and 0.8 Mach and rolls of 1 and 3 degrees were considered to investigate the roll. In this state, a deflection was applied on the control fins, resulting in a pure roll in the models.

Figure 34 depicts a diagram of the roll moment coefficient based on the deflection angle at a speed of 0.6 Mach.

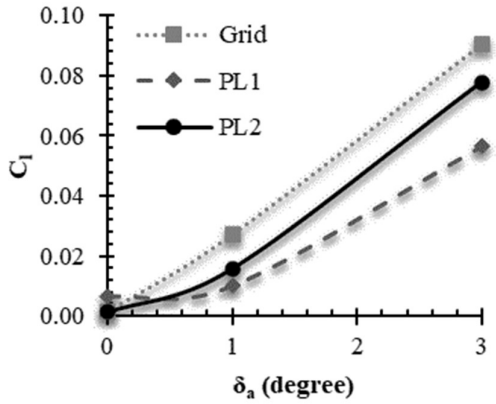

Figure 34. Diagram for roll moment coefficient (C_l) at Mach 0.6.

The above figure shows how many moments are created for each degree of the roll. This indicates that the model Grid creates more roll moments for constant deflection than other models, which causes the superiority of this model over PL1 and PL2 models. Considering the previous investigations, due to the small chord of PL2 compared to PL1, the upstream flow passes mainly over one side of the wing. As a result, the model PL2 creates more roll moments than PL1. A diagram of the roll moment at 0.7 Mach is shown in Figure 35 to confirm the above-mentioned points. Figure 35 demonstrates the points mentioned above at a Mach number of 0.7. For a more precise investigation, the aforementioned roll moment at a speed of 0.8 Mach is depicted in Figure 36.

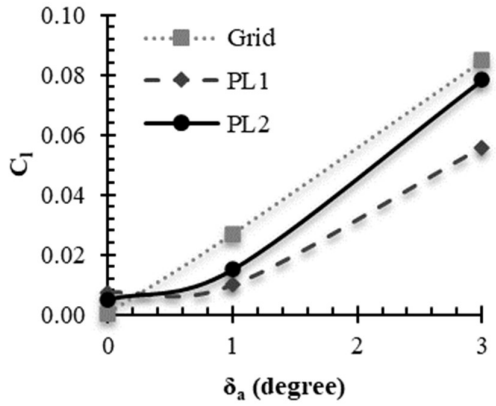

Figure 35. Diagram for inductive roll moment coefficient (C_l) at Mach 0.7.

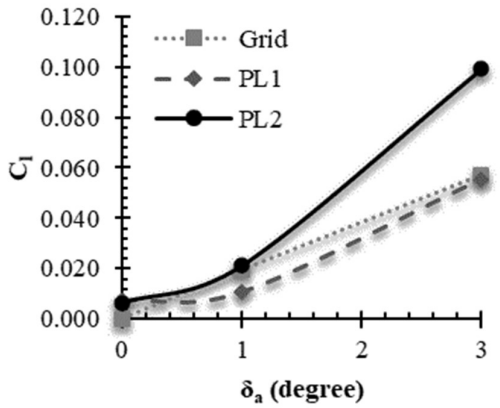

Figure 36. Diagram for inductive roll moment coefficient (C_l) at Mach 0.8.

Figure 36 repeats the procedure of the previous diagrams, except that the model Grid's roll moment has declined. For a more precise investigation of this issue, the speed streamline shape has been depicted in Figure 37, which is the internal view of the grid fin. It shows that the speed within the grid lattices has reached 1 Mach, causing the flow to choke inside them. This would result in a declination of the flow, leading to a reduction of the moment coefficient in Figure 36.

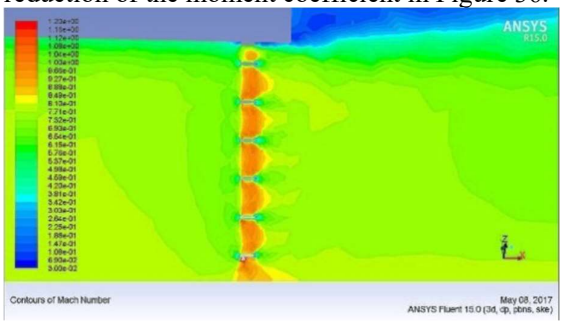

Figure 37. Speed streamline shape of model Grid at Mach 0.8.

The effects of these variations are also investigated. As previously mentioned, it is necessary to have a trim angle and balance of the forces and moments for an aircraft to fly. The trim angle requires a positive pitch so that the aircraft's nose is upward. Regarding the previously mentioned effects, this would create an inductive roll in the aircraft. This is why applying a negative roll on the control fins neutralizes the effect of this phenomenon.

Furthermore, a more maneuverable aircraft, which is more suitable for the designer, has lower induced roll during the flight. Because neutralizing this effect by negative roll would cause a part of the control fin's motion range to be spent for neutralizing the effect of this phenomenon. At the same time, it could be utilized for better control of the aircraft and used in the following maneuvers. On this basis, the investigation and analyses were performed to select a model with less affectability and better maneuverability during the flight. The roll required for neutralization of this effect can be calculated regarding the obtained results and using the superposition principle. If it is assumed that all the models are flying with a Mach number of 0.7, then they will need a 3-degree pitch for trimming. According to the obtained data, the value of inductive roll based on the control fin's pitch angle for each model is described in Table 5.

Table 5 Inductive roll values(degree) of each model at speed of 0.7 Mach

PL2	PL1	Grid	$CMx - 0/\mathrm{De}$ (dgree)
0.0022	0.0055	0.0007	

Now, based on the roll data of each model for 1° angle, the value of the roll angle required by the control fins for neutralizing this effect can be calculated. Table 6 represents the roll value based on the roll angle of the control fin. Based on the above values, the required roll angle values are represented in Table 7. Based on Table 7, it can be concluded that, as shown in Figure 29, 30, and 33, the model Grid has the lowest affectability and requires nearly 0.025 degrees for neutralizing the effect of inductive roll, which is provided by the control fin. Next is the model PL2, where almost 0.2 degrees of the control fin's turning would be allocated to neutralizing the inductive roll's effect. However, in model PL1, this value reaches almost 0.5 degrees. This constraint exists for all the models. Now, if the trim requires more pitch or increased speed, this value will be increased, which will cause serious constraints in the control of the models during flight as well as in the maneuverability of the aircraft. One of the advantages of the model Grid is that it has less affectability compared to other models.

Table 6 Roll values(degree) at 1° angle of models

PL2	PL1	Grid	$CMx - 0/\mathrm{Da}$ (degree)
0.015	0.01	0.027	

Table 7 Angle(degree) values for neutralizing in each model at 0.7 Mach

PL2	PL1	Grid	D_a (degree)
0.146	0.55	0.025	

Conclusion

In the present paper, three given models were studied in terms of control and static stability by selecting the appropriate model of turbulence and mesh independence. The affectability of the three selected models with different stabilizer wings from the upstream flow during pitch and roll was investigated. The results in the pitching aspect show that the Grid model has better static stability due to its physical nature (static margin number 1) and a lower induction roll than other models.

In the Grid model, the induction roll is 68% less than model PL2, and PL2 has an induction roll of 60% less than PL1 due to its lower surface area. In the case of using a control wing to neutralize the induction roll, the Grid model uses it 82% less than the PL2, and the PL2 model applies it 73% less than the PL1 model.

Furthermore, the model PL2 wight has a smaller wing chord than PL1 could be a more appropriate choice up to the pitch of 3 degrees, but the pitch of 6 degrees and over it faces a severe induced roll.

Analyses indicate that its small chord causes to be influenced by the upstream current severely because a lot of side force is pleased in it.

As for the pitch channel, the Grid model was the best choice at Mach numbers of 0.6 and 0.7 and could help this channel; however, at 0.8 Mach, due to choking of the flow inside the lattice, a moment loss occurred in the grid fin. As for the control of the given model, it could be concluded that the Grid model had the best maneuverability due to its lower affectability in the inductive roll. As a result, it could have appropriate conditions in all of the given states due to its physical nature.

References

[1] Washington, W.D. and M.S. Miller, "Grid fins - a new concept for missile stability and control.", 31st AIAA aerospace sciences meeting, Reno, USA, (1993, January).

[2] Washington, W.D. and M.S. Miller, "Experimental investigations of grid fin aerodynamics: A synopsis of nine wind tunnel and three flight tests", Proceedings of RTO AVT Symposium on missile aerodynamics, Sorrento, Italy, (1998, May).

[3] DeSpirito, J. and J. Sahu, "Viscous CFD calculations of grid fin missile aerodynamics in the supersonic flow regime.", 39th AIAA aerospace sciences meeting and exhibit, Reno, USA, (2001, January).

[4] Hughson, M.C., E.L. Blades, and G.L. Abate, "Transonic aerodynamic analysis of lattice grid tail fin missiles", 24th AIAA applied aerodynamics conference, San Francisco, USA, (2006).

[5] Zeng, Y., J. Cai, M. Debiasi, and T.L. Chng, "Numerical study on drag reduction for grid-fin configurations", 47th AIAA aerospace sciences meeting, Orlando, USA, (2009, January).

[6] Munawar, S, "Analysis of grid fins as efficient control surface in comparison to conventional planar fins", 27th international congress of the aeronautical sciences, Nice, France, (2010, September).

[7] Bak, M., "Experimental investigation and computational fluid dynamics analysis of missile with grid fin in subsonic flow", International Journal of Engineering Science and Technology, 2(11):6214-6220, (2010).

[8] Kless, J.E. and M.J. Aftosmis, "Analysis of grid fins for launch abort vehicle using a Cartesian Euler solver", 29th AIAA applied aerodynamics conference, Honolulu, USA, (2011).

[9] Prashanth, H., Ravi K. S., Krishnappa G. B., "Aerodynamic Characteristics of G16 Grid Fin Configuration at Subsonic and Supersonic Speeds", International Journal of Engineering Research and General Science Volume 2, Issue 5, pp. 129-135, (2014).

[10] Landers, M.G., L.H. Hall, and L.M. Aumar, "Aerodynamic predictions of pitch and roll control for canard-controlled missiles", 18th AIAA applied aerodynamics conference, Denver, USA, (2000, August).

[11] DeSpirito, J., M.E. Vaughn, and W.D. Washington, "CFD investigation of canard-controlled missile with planar and grid fins in the supersonic flow". AIAA atmospheric flight mechanics conference and exhibit, Monterey, USA, (2002, August).

[12] DeSpirito, J., M.E. Vaughn, and W.D. Washington, "Numerical investigation of aerodynamics of canard-controlled missile using planar and grid tail fins, part ii: subsonic and transonic flow". U.S. Army Research Laboratory Aberdeen proving ground ARL-TR-3162, (2004).

[13] Pruzan, D.P., M.R. Mendenhall, and W.C. Rose, Schuster D.M., "Grid Fin Stabilization of the Orion Launch Abort Vehicle". 29th AIAA applied aerodynamics conference, Honolulu, USA, (2011, June).

[14] DeSpirito, J., M.E. Vaughn, and W.D. Washington, "Numerical investigation of canard-controlled missile

with planar and grid fins". Journal of Spacecraft and Rockets, 40 (3): 363-370, (2003).

[15] Khalid M., Sun Y., Xu H., "Computation of Flows Past Grid Fin Missiles, in: Missile Aerodynamic.", RTO MP-5, Sorrento, Italy, pp. 11–14, (1998).

[16] Ledlow, T., Burkhalter, J., and Hartfield, R., "Integration of Grid Fins for the Optimal Design of Missile Systems", AIAA Atmospheric Flight Mechanics Conference, Kissimmee, Florida, (2015).

[17] Dincer, E., "Aerodynamic design and performance analyses of grid fin in supersonic flow using design of experiments and computational fluid dynamics", Thesis M.Sc., Ankara, Turkey, (2022).

[18] Hoffman, J. and Johnson, C., "Computational Turbulent Incompressible Flow", Springer, Berlin, Germany, (2006).

[19] Cai, J., "Numerical study on choked flow over grid-fin configurations", Journal of Spacecraft and Rockets 46(5):949-956, (2009).

[20] Theerthamalai, P. and N. Balakrishnan, "Effect of geometric parameters on the aerodynamic characteristics of grid-fin cells at supersonic speeds", 45th AIAA aerospace sciences meeting and exhibit, Reno, USA, (2007, January).

[21] Abate, G.L., R.P. Duckerschein, and W. Hathaway, "Subsonic/transonic free-flight tests of a generic missile with grid fins", 38th AIAA aerospace sciences meeting and exhibit, Reno, USA, (2000, January).